





X-ray standing waves reveal lack of OH termination at hydroxylated ZnO(0001) surfaces

Jens Niederhausen ^{1,*} Antoni Franco-Cañellas ² Simon Erker,³ Thorsten Schultz,¹ Katharina Broch,² Alexander Hinderhofer,² Steffen Duhm ⁴ Pardeep K. Thakur,⁵ David A. Duncan,⁵ Alexander Gerlach,² Tien-Lin Lee,⁵ Oliver T. Hofmann,³ Frank Schreiber ² and Norbert Koch¹

¹Helmholtz-Zentrum Berlin für Materialien und Energie GmbH, 12489 Berlin, Germany
and Humboldt-Universität zu Berlin, Institut für Physik & IRIS Adlershof, 12489 Berlin, Germany

²Institut für Angewandte Physik, Universität Tübingen, 72076 Tübingen, Germany

³Institut für Festkörperphysik, Graz University of Technology, NAWI Graz, 8010 Graz, Austria

⁴Institute of Functional Nano & Soft Materials (FUNSOM), Jiangsu Key Laboratory for Carbon-Based Functional Materials and Devices, Soochow University, Suzhou, Jiangsu 215123, People's Republic of China

⁵Diamond Light Source, Harwell Science and Innovation Campus, Oxfordshire OX11 0DE, United Kingdom



(Received 26 February 2019; revised manuscript received 18 August 2019; accepted 15 January 2020; published 28 February 2020)

The vertical adsorption distances of the planar conjugated organic molecule 3,4,9,10-perylenetetracarboxylic diimide (PTCDI) on hydroxylated ZnO(0001), determined with the x-ray standing wave technique (XSW), are at variance with adsorption geometries simulated with density functional theory for surface-structure models that consider terminating OH, whereas good agreement is found for PTCDI in direct contact with the topmost Zn layer. The consequential assignment of OH to subsurface sites is supported by additional, independent XSW and energy scanned photoelectron diffraction data and calls for a reconsideration of the prevalent surface models with important implications for the understanding of ZnO(0001) surfaces.

DOI: [10.1103/PhysRevMaterials.4.020602](https://doi.org/10.1103/PhysRevMaterials.4.020602)

The surface structure of zinc oxide (ZnO) exposed to water (H₂O) and hydrogen (H, H₂) is important not only for the understanding of heterogeneous catalytic processes [1–5] but also because it controls the morphologies of condensed water [6] and organic or metal adlayers [7,8], which are relevant for self-cleaning and (opto)electronic applications, respectively. Hydroxyl (OH) formation is generally found in these cases [9–12]. Zn-polar ZnO(0001) (Zn-ZnO) is the only ZnO facet that does not feature oxygen atoms in the surface layer. Therefore, OH formation is particularly intriguing in this case and pinpointing the OH location is very relevant.

In a purely ionic treatment, a stoichiometric Zn-ZnO surface carries an extra positive 0.5 elementary charge per surface Zn atom that gives rise to a divergent surface energy. Neutral surfaces can be achieved with surface stoichiometries that have 0.25 monolayers (ML) less Zn than O atoms in the form of defects and/or surface reconstructions [5,13,14]. Indeed, stoichiometric surfaces have not been observed by scanning probe microscopy (SPM). Hitherto resolved structures can be roughly separated in microscopically reconstructed but macroscopically flat surface areas [15–17] and areas that are reconstructed into triangular islands and holes (and thus

macroscopically rough) and additionally exhibit high densities of vacancies and pits [13,15,17–21]. The presence of OH at the surfaces investigated in these SPM measurements is expected even if the samples were not intentionally exposed to water or hydrogen [5], because under typical UHV conditions, residual H₂O and H₂, as well as atomic H created by the pressure gauge filament and/or ion getter pump, [7,18,22] amount to nonintentional doses of 1 langmuir (L) on the timescale of a few hours. Consistently, in the current work and in previous studies [11,17,23] OH was observed for samples nonintentionally exposed using x-ray photoelectron spectroscopy (XPS). Strikingly though, on-surface OH formation has so far not been seen by SPM. Protrusions were reported, but an assignment to OH was implicitly [16] or explicitly [21] dismissed by the authors. The SPM data thus hint at OH in subsurface sites. This configuration has indeed been proposed by Valtiner *et al.* based on first-principles thermodynamics adjusted *ad hoc* to include kinetically stabilized surface reconstructions [24].

A problem with SPM of Zn-ZnO is that only a part of the surface area can be unambiguously determined [15,16,19]. This experimental uncertainty and results from earlier calculations [5,14] can explain why predominately OH-terminated Zn-ZnO surfaces are assumed when rationalizing results from spectroscopy and diffraction experiments [10,11,14,23,25–27]. In view of the inherent limitations of first-principles thermodynamics [14,24,28], novel experimental approaches are required to conclusively test the notion of OH-terminated Zn-ZnO.

To this end, we determine interatomic vertical distances of hydroxylated Zn-ZnO with the x-ray standing wave (XSW)

*jens.niederhausen@helmholtz-berlin.de

Published by the American Physical Society under the terms of the Creative Commons Attribution 4.0 International license. Further distribution of this work must maintain attribution to the author(s) and the published article's title, journal citation, and DOI.

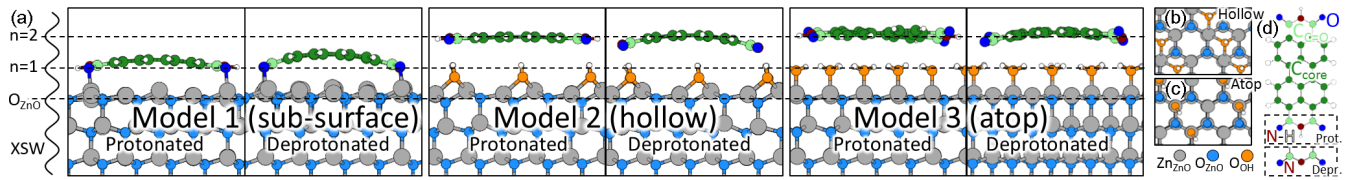


FIG. 1. (a) Calculated geometries for Zn-ZnO surface models 1–3 and protonated and deprotonated PTCDI using DFT [29]. The x-ray standing wave (XSW) is included to illustrate the ambiguity of the vertical adsorption distances determined with the XSW technique. The height of the O_{ZnO} layer, used as reference in Table II and Figs. 2(b) and 3(a), is also indicated. (b), (c) Top view of models 2 and 3 that feature 0.5 ML OH in hollow and atop sites, respectively. (d) PTCDI's chemical structure and effect of deprotonation.

technique [30,31] and compare these with the corresponding distances determined with density functional theory (DFT, see Ref. [29] for details) for clean Zn-ZnO (model 1, implicitly limiting OH to subsurface sites) and OH-terminated Zn-ZnO. Because of the exclusive sensitivity to molecule-surface vertical distances in normal-incidence XSW (NIXSW) measurements presented later on, we test the least and most protruding OH configurations for OH-terminated Zn-ZnO, namely (2×1) -OH overlayers in fcc hollow [3,5,14,23,32] (model 2) and atop sites [1] (model 3) [cf. Figs. 1(b) and 1(c)].

The NIXSW analysis [29] of the partial photoelectron yield stemming from chemical species X yields the coherent position $P_{H,X}$ and coherent fraction $f_{H,X}$ that quantify its location within the standing wave field and its positional disorder, respectively. The vertical distance between X and an arbitrary reference species Y can then be calculated according to $d_{X,Y} = d_H(n + P_{H,Y} - P_{H,X})$, where $d_H = 2.602 \text{ \AA}$ is the diffraction plane spacing of ZnO for $H = (0002)$ and $n = 0, 1, 2, \dots$ is a free parameter that reflects the fact that XSW is only sensitive to the vertical position with respect to H modulo the period of the standing wave field. Importantly, several effects sensitively influence f_H [30,33–35] and effects beyond the current theoretical description are indicated by observed f_H variations between different chemical elements [33] and chemical species of the same element [34]. P_H is a much more robust observable.

The O 1s core-level signal for oxygen in ZnO (O_{ZnO}) and OH (O_{OH}) can be separately resolved by XPS [29], allowing us to determine the unknown location of O_{OH} with respect to the substrate crystal structure, as is common XSW practice. In the current case, however, this approach suffers from two intricacies: Firstly, model 1 does not explicitly include OH and does not permit a direct comparison with experiment. Secondly, due to the finite information depth of XPS, near-surface d_H variations due to surface relaxation and surface preparation-induced effects have to be accounted for.

As we will show below, a convincing case based on precise $d_{O_{ZnO}, O_{OH}}$ values is nonetheless possible if also including XSW data obtained from a nonspecular reflection as well as energy scanned photoelectron diffraction (PhD) data. However, in order to increase the confidence in this assessment, we additionally followed an independent NIXSW-based approach: We deposit the planar π -conjugated organic molecule (COM) 3,4,9,10-perylenetetracarboxylic diimide [PTCDI, see Fig. 1(d)] and test whether PTCIDI adsorbs on top of terminating OH and, in turn, whether the O_{OH} location is above or below the topmost Zn layer. XSW would sense this (I) from OH acting

as spacer layer between PTCIDI and Zn-ZnO and (II) via the O_{OH} -PTCDI distances. These additional measurements address both problems laid out above: First, approach (I) relies on distances between PTCIDI and Zn-ZnO and an explicit knowledge of the OH location is not required, allowing to also test model 1. Second, for an assumed OH termination, all O_{OH} would be localized in the surface layer and directly in contact with PTCIDI. Therefore, approach (II) is not affected by d_H variations in the Zn-ZnO surface crystal structure. The Zn-ZnO surfaces were prepared according to three different recipes (labeled A–C) that represent the range of annealing temperatures employed in most previous Zn-ZnO surface studies [7,13,15,17,18,20,22,36,37] and also include H_2O exposure [37]. All crystals were hydrothermally grown (CrysTec, Berlin), annealed under atmospheric conditions (1000 °C, 2 h) and *in-situ* (420 °C, 10 min), and Ar^+ sputter-cleaned (0.5 keV, 15 min) [29]. Final annealing temperatures $T_{ann.}$ are included in Table I. For sample C, we monitored the OH fingerprint in the O 1s spectrum to elucidate the OH dynamics under UHV conditions and the effect of H_2O exposure. We could confirm complete OH desorption during annealing [29] and Fig. 2(a) shows a gradual re-formation of OH in the UHV environment as well as similar saturation OH intensities within the explored H_2O partial pressure range from $<3 \times 10^{-10}$ mbar (= UHV base pressure) to 5×10^{-8} mbar.

Table I reports all relevant NIXSW results. As shown in Ref. [29], increasing f_H when comparing samples A–C results from surface order being initially reduced by sputter-induced

TABLE I. NIXSW results [29]. Scans before (after) PTCIDI deposition were used for the substrate signals for samples A and B (sample C). The f_H (P_H) uncertainty is estimated to be ± 0.1 (± 0.01) for O_{ZnO} and Zn_{ZnO} and ± 0.03 for all other data) except for ± 0.2 (± 0.05) for the N signal in the case of sample C due to a slight initial N contamination [29].

Sample ($T_{ann.}$)	A (420 °C)		B (600 °C)		C (700 °C)	
	P_H	f_H	P_H	f_H	P_H	f_H
O_{ZnO}	0.88 ^a	0.81	0.81	0.89	0.78	0.95
O_{OH}	0.78	0.54	0.63	0.60	0.65	0.62
Zn_{ZnO}	0.09 ^a	0.85	0.03	0.98	0.00	1.01
N	0.87	0.55	0.81	0.81	0.74	1.07
$C_{C=O}$	0.97	0.65	0.92	0.80	0.87	0.71
C_{core}	0.11	0.28	0.15	0.35	1.00	0.55

^aCorrected for surface relaxation by +0.02 [29].

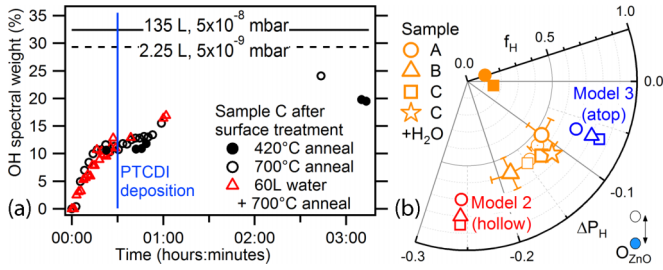


FIG. 2. (a) OH spectral contribution derived from O 1s core-level fits [29] as a function of time after the respective annealing was stopped. Horizontal lines show OH spectral weights directly after the indicated H₂O doses and corresponding partial pressures. The vertical line indicates when PTCDI was deposited onto sample C. (b) Experimentally determined ΔP_H (referenced to O_{ZnO}) and f_H for O_{OH} (orange) and the corresponding theoretical values for surface models 2 and 3 (red and blue). The data are presented by employing ΔP_H as angle and f_H as radius. The star corresponds to sample C after H₂O-dosing. The samples discussed in [29] are symbolized as thin circles (thin squares) if annealed at 420 °C (700 °C). Filled symbols show results for the (10 $\bar{1}$ 1) reflection. The three f_H values for models 2 and 3 approximate the surface disorder of samples A–C (see text).

damage/Ar-implantation and consecutively restored during annealing to a degree that depends on T_{ann} , and the annealing duration. Vertical disorder in the topmost Zn layer additionally contributes. We derive $f_H = 0.7, 0.8,$ and 0.85 for the topmost Zn layer of samples A, B, and C, respectively. The respective lower $f_{H,\text{O}_{\text{OH}}}$ indicates OH vertical disorder beyond that of the topmost Zn layer. The DFT-calculated vertical distances d are presented in Table II and can be converted into coherent positions via d/d_0 . The coherent position of another species can be selected as reference plane (denoted $P_{H,Y}$), converting $P_{H,X}$ to $\Delta P_{H,X} = P_{H,X} - P_{H,Y}$. The Argand diagram [38] in Fig. 2(b) employs $X = \text{O}_{\text{OH}}$ and $Y = \text{O}_{\text{ZnO}}$ and thus $\Delta P_{H,\text{O}_{\text{OH}}} = 0$ corresponds to O_{OH} at the same vertical position as O in the ZnO lattice. The presented comparison between experimental and theoretical values shows that model 2 is clearly at variance with experiment. In contrast, $d_{\text{O}_{\text{ZnO}},\text{O}_{\text{OH}}}$ predicted by model 3 is consistent with most of the NIXSW data if we additionally allow for a possible inward surface relaxation that we estimate as $P_{H,\text{relax.}} \leq 0.04$ (i.e., 0.1 Å) [29]. However, it seems that O_{OH} in bridge sites [23,32] or a combination of adsorption sites would potentially fit the NIXSW results better. To test these options further, we

TABLE II. DFT-calculated vertical adsorption distances (in Å) of PTCDI and OH for models 1–3 and for protonated and deprotonated PTCDI, measured from the topmost oxygen layer of the ZnO crystal.

Model (OH site)	1 (subsurf.)		2 (hollow)		3 (atop)	
	Prot.	Depr.	Prot.	Depr.	Prot.	Depr.
PTCDI state						
N	2.78	2.55	5.10	4.51	5.37	5.01
C _{C=O}	2.86	2.81	5.09	4.69	5.38	5.17
C _{core}	3.21	3.45	5.20	5.26	5.48	5.50
O _{OH}			1.93	1.92	2.43	2.43

performed PhD to probe the local geometric structure of O_{OH}. Furthermore, we conducted XSW with $H = (10\bar{1}1)$ as diffraction plane to gain access to O_{OH}'s in-plane atomic coordinates. The PhD results are presented in Ref. [29] and point to O_{OH} in O_{ZnO}-like sites, but with a higher degree of disorder. This site assignment excludes a significant abundance of OH in hollow (model 2) or bridge sites, leaving model 3 with its near O_{ZnO}-like atop site as the only realistic option for OH-terminated Zn-ZnO. However, in the XSW data for the (10 $\bar{1}$ 1) reflection that is included in Fig. 2(b), a very high degree of in-plane disorder is apparent from the low f_H . This is not consistent with the notion of a single atop site dominating the OH population as would be the case for model 3. In addition, the atop configuration should be inherently unstable [3,5,14]. Indeed, in our DFT calculations we have to constrain the O_{OH} to stay on top of surface Zn atoms, because otherwise they relax into the energetically more favorable model 2 configuration. Therefore we suggest that OH, instead, substitutes subsurface oxygen sites, e.g., next to Zn vacancies and along the edges of surface reconstructions as suggested in Refs. [17,23] and Ref. [24], respectively. In this case, O_{OH} likely occupies a large variation of near O_{ZnO}-like sites, explaining also the in-plane disorder.

To substantiate these findings, we turn to the measurements that employ PTCDI as surface-structure probe. ZnO crystals have been probed by means of molecular adsorbates before: In a pioneering work, Staemmler *et al.* measured the binding energy of CO with thermal desorption spectroscopy and could successfully resolve several ZnO surface structures [39]. However, for hydroxylated Zn-ZnO surfaces, the authors could detect “no adsorption of CO [...] even at surface temperatures as low as 50 K,” leaving the OH location at Zn-ZnO surfaces an open question [5,24].

Our XSW-based approach differs from that of Staemmler *et al.* in two aspects: First, PTCDI is a much larger surface-structure probe than CO and adsorption at room temperature is guaranteed. On the other hand, the interaction with oxide surfaces is more complex for large COMs than for CO. XPS yields significant chemical shifts of PTCDI's C 1s and N 1s core levels at the PTCDI/ZnO interface compared to bulklike PTCDI. From ultraviolet photoelectron spectroscopy (UPS), additional occupied density of states in the gap between highest occupied and lowest unoccupied molecular orbital (HOMO and LUMO) in the interface regime is apparent [27,29,40]. These observations are equivalent to those reported for PTCDI/TiO₂, for which a deprotonation reaction of PTCDI at the oxide surface was suggested as possible origin [41]. However, the same observations were also reported for C₄-PTCDI on ZnO [27], for which the N atoms are bound to butyl groups and a deprotonation reaction is not possible. Charge transfer rather than a change of PTCDI's chemical structure was thus proposed to explain the chemical shifts [27,40]. To account for this uncertainty, we performed DFT calculations for models 1–3 for both protonated and deprotonated PTCDI, assume a coexistence of both states possible, and consider the adsorption distances between those resulting for protonated and deprotonated PTCDI as possibility space.

Second, the unclear concentration and type(s) of intrinsic dopants in ZnO yields large uncertainties for calculated COM

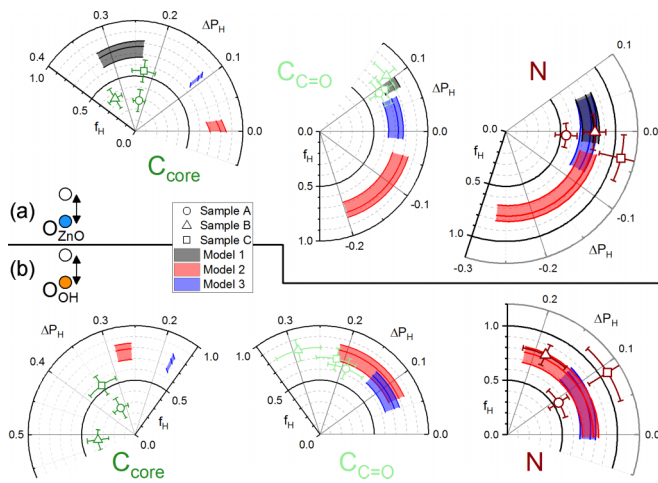


FIG. 3. (a) Experimentally determined ΔP_H (referenced to O_{ZnO}) and f_H for the PTCDI signals. The corresponding theoretical results are shown as filled areas that connect ΔP_H for protonated and deprotonated PTCDI for each model. Lines account for the surface disorder of, from inner to outer, samples A–C. (b) The same as (a) but referenced to O_{OH} .

binding energies. Assuming, e.g., zinc interstitials instead of oxygen vacancies as dopants was found to change the binding energy of protonated PTCDI/ZnO from 2.3 eV to 1.1 eV [40]. We prevent this problem by exclusively relying on PTCDI's adsorption distances. These were shown to be barely affected when going from stoichiometric to doped surfaces as well as when changing dopant type and location [40].

As can be seen from our and previous UPS results [27,29,40], PTCDI wets the Zn-ZnO surface particularly well. In addition, PTCDI's footprint is too large to fit into the small Zn-ZnO surface openings (pits, rows and stripes of missing atoms, vacancies) but still small compared to most of the flat parts of the macroscopically rough surface areas. These are important prerequisites for probing a large fraction of the surface area and arriving at results that are truly representative of the Zn-ZnO surface structure.

PTCDI films of low sub-ML coverage and approximately ML coverage were deposited from a custom-built Knudsen cell onto samples A and B, respectively, ~ 4 hours after they had undergone their final annealing. As can be extrapolated from our OH-vs-time analysis in Fig. 2(a), this marks enough time to approximately saturate their surfaces with OH. In contrast, the time was reduced to only 30 min for sample C to increase the chance that a relevant fraction of PTCDI adsorbs onto OH-free surface patches. From the data in Fig. 2(a), we estimate that the surface of sample C was OH-depleted by 50% during PTCDI deposition compared to samples A and B. Photoelectron yields could be separately resolved for PTCDI's carbonyl C ($C_{C=O}$) and N (both representative of PTCDI's functional groups) and all other C (C_{core} , representative of its perylene core). PTCDI's $O_{C=O}$ has a core-level binding energy very similar to O_{OH} and a XSW-analysis is not reliably possible [29]. As motivated above, we follow two different approaches, each employing an independent reference plane.

(i) Starting by first using O_{ZnO} as reference [Fig. 3(a)], a significant intramolecular bending is apparent for all three samples from the ΔP_H differences between C_{core} , $C_{C=O}$,

and N. As can be seen in Fig. 1(a), this finding is in contrast to models 2 and 3 when assuming protonated PTCDI but approximately consistent with all other cases. However, when also considering the *absolute* ΔP_H values, models 2 and 3 are clearly incompatible with the experimental data for C_{core} and, to a smaller degree, $C_{C=O}$. In contrast, very good agreement between theory and experiment is achieved for model 1. Two aspects deserve special attention: First, the larger $\Delta P_{H,C_{core}}$ for sample B than samples A and C can be rationalized by an increased intermolecular interaction at the larger PTCDI coverage in this case [29], a correlation that was reported for pentacene on Ag(111) [42]. In contrast, the OH depletion of the surface of sample C has no apparent effect on the adsorption distances that could, in turn, be related to terminating OH. Second, while the observed lower f_H for C_{core} than for $C_{C=O}$ and N is qualitatively consistent with bent molecules, experimental and theoretical $f_{H,C_{core}}$ do not agree within the error bars. A coexistence of different PTCDI chemical [41] or charge states [40], as indicated by two nitrogen species found from XPS [27,29,41], and a fraction of PTCDI in contact with H [16] or oxygen adatoms [21] are possible reasons for the relatively low $f_{H,C_{core}}$.

(ii) From Fig. 3(b) it is clear that models 2 and 3 do not match the experiment also when using O_{OH} as reference. The discrepancy is least (most) pronounced for model 2 (3) due to a vertical (almost horizontal) OH bond orientation [cf. Fig. 1(a)].

Summarizing our conclusions from (i) and (ii), models 2 and 3 predict significantly too low adsorption heights, with the deviation for model 2 (3) being largest when referenced to O_{ZnO} (O_{OH}). Since our analysis covered the most and least protruding OH sites, this assessment also holds for intermediate terminating OH configurations like in bridge sites.

This is clear experimental evidence that an OH termination, even though predicted as thermodynamically most stable [5,14], does in fact not form upon Zn-ZnO hydroxylation in UHV. This suggests that kinetic barriers preserve the reconstructions that stabilize OH-free Zn-ZnO surfaces [13], as previously proposed by Valtiner *et al.* [24]. Since a comprehensive quantum-chemical description of the dynamic equilibrium of Zn-ZnO surface structures at realistic pressures and temperatures is still out of reach, only selected adsorption pathways [43,44] and surface configurations [32] have been tested. The present results demonstrate the importance of considering subsurface OH sites and modeling their formation and stabilization.

In conclusion, we have introduced a scheme to determine surface structures via the vertical adsorption distances of planar molecules and exploit this method to probe hydroxylated Zn-ZnO surfaces with PTCDI. The geometric structure prediction of PTCDI/Zn-ZnO warrants a sensitive comparison with experiment because the adsorption distances are primarily determined by the OH group configuration. Our results are not consistent with the common notion of OH-terminated Zn-ZnO surfaces but strongly hint towards OH in subsurface sites with significant in-plane disorder. This finding will have great implications for surface chemistry and heterogeneous catalysis and hopefully inspire increased incorporation of kinetic effects in theoretical modeling of surface structures, ultimately allowing their adequate description under realistic conditions.

The authors thank the Diamond Light Source for access to beamline I09 (beamtimes SI11415-1, SI13740-1, and SI19033-1), D. McCue for excellent technical support, as well as Q. Wang and M.-T. Chen for their help during the beamtime. J.N. thanks Georg Heimel for inspiring discussions. O.T.H. and S.E. acknowledge FWF P27868 and P28631. J.N. and T.S. acknowledge funding by the Deutsche

Forschungsgemeinschaft (DFG)–Project-ID 182087777–SFB 951. S.D. acknowledges the 111 Project of the Chinese State Administration of Foreign Experts Affairs, the Collaborative Innovation Center of Suzhou Nano Science & Technology (NANO-CIC), and the Soochow University–Western University Joint Center for Synchrotron Radiation Research.

-
- [1] A. Wander and N. M. Harrison, The stability of polar oxide surfaces: The interaction of H_2O with $\text{ZnO}(0001)$ and $\text{ZnO}(000\bar{1})$, *J. Chem. Phys.* **115**, 2312 (2001).
- [2] C. Wöll, Hydrogen adsorption on metal oxide surfaces: a reinvestigation using He-atom scattering, *J. Phys.: Condens. Matter* **16**, S2981 (2004).
- [3] B. Meyer, First-principles study of the polar O-terminated ZnO surface in thermodynamic equilibrium with oxygen and hydrogen, *Phys. Rev. B* **69**, 045416 (2004).
- [4] C. Wöll, The chemistry and physics of zinc oxide surfaces, *Prog. Surf. Sci.* **82**, 55 (2007).
- [5] G. Kresse, O. Dulub, and U. Diebold, Competing stabilization mechanism for the polar $\text{ZnO}(0001)$ -Zn surface, *Phys. Rev. B* **68**, 245409 (2003).
- [6] M. M. Gentleman and J. A. Ruud, Role of hydroxyls in oxide wettability, *Langmuir* **26**, 1408 (2010).
- [7] O. Dulub, L. A. Boatner, and U. Diebold, STM study of Cu growth on the $\text{ZnO}(10\bar{1}0)$ surface, *Surf. Sci.* **504**, 271 (2002).
- [8] B. Meyer and D. Marx, Density-functional study of Cu atoms, monolayers, films, and coadsorbates on polar ZnO surfaces, *Phys. Rev. B* **69**, 235420 (2004).
- [9] H. Noei, H. Qiu, Y. Wang, E. Löffler, C. Wöll, and M. Muhler, The identification of hydroxyl groups on ZnO nanoparticles by infrared spectroscopy, *Phys. Chem. Chem. Phys.* **10**, 7092 (2008).
- [10] M. Valtiner, S. Borodin, and G. Grundmeier, Preparation and characterisation of hydroxide stabilised $\text{ZnO}(0001)$ -Zn-OH surfaces, *Phys. Chem. Chem. Phys.* **9**, 2406 (2007).
- [11] R. Heinhold, G. T. Williams, S. P. Cooil, D. A. Evans, and M. W. Allen, Influence of polarity and hydroxyl termination on the band bending at ZnO surfaces, *Phys. Rev. B* **88**, 235315 (2013).
- [12] B. S. Mun, Z. Liu, M. A. Motin, P. C. Roy, and C. M. Kim, In situ observation of H_2 dissociation on the $\text{ZnO}(0001)$ surface under high pressure of hydrogen using ambient-pressure XPS, *Int. J. Hydrogen Energy* **43**, 8655 (2018).
- [13] O. Dulub, U. Diebold, and G. Kresse, Novel Stabilization Mechanism on Polar Surfaces: $\text{ZnO}(0001)$ -Zn, *Phys. Rev. Lett.* **90**, 016102 (2003).
- [14] M. Valtiner, M. Todorova, G. Grundmeier, and J. Neugebauer, Temperature Stabilized Surface Reconstructions at Polar $\text{ZnO}(0001)$, *Phys. Rev. Lett.* **103**, 065502 (2009).
- [15] J. Dumont, B. Hackens, S. Faniel, P.-O. Mouthuy, R. Sporken, and S. Melinte, $\text{ZnO}(0001)$ surfaces probed by scanning tunneling spectroscopy: Evidence for an inhomogeneous electronic structure, *Appl. Phys. Lett.* **95**, 132102 (2009).
- [16] S. Torbrügge, F. Ostendorf, and M. Reichling, Stabilization of zinc-terminated $\text{ZnO}(0001)$ by a modified surface stoichiometry, *J. Phys. Chem. C* **113**, 4909 (2009).
- [17] M. Hellström, I. Beinik, P. Broqvist, J. V. Lauritsen, and K. Hermansson, Subsurface hydrogen bonds at the polar Zn-terminated $\text{ZnO}(0001)$ surface, *Phys. Rev. B* **94**, 245433 (2016).
- [18] O. Dulub, L. A. Boatner, and U. Diebold, STM study of the geometric and electronic structure of $\text{ZnO}(0001)$ -Zn, $(000\bar{1})$ -O, $(10\bar{1}0)$, and $(11\bar{2}0)$ surfaces, *Surf. Sci.* **519**, 201 (2002).
- [19] F. Ostendorf, S. Torbrügge, and M. Reichling, Atomic scale evidence for faceting stabilization of a polar oxide surface, *Phys. Rev. B* **77**, 041405(R) (2008).
- [20] J. H. Lai, S. H. Su, H.-H. Chen, J. C. A. Huang, and C.-L. Wu, Stabilization of ZnO polar plane with charged surface nanodefects, *Phys. Rev. B* **82**, 155406 (2010).
- [21] H. Xu, L. Dong, X. Q. Shi, M. A. Van Hove, W. K. Ho, N. Lin, H. S. Wu, and S. Y. Tong, Stabilizing forces acting on ZnO polar surfaces: STM, LEED, and DFT, *Phys. Rev. B* **89**, 235403 (2014).
- [22] T. Becker, S. Hövel, M. Kunat, C. Boas, U. Burghaus, and C. Wöll, Interaction of hydrogen with metal oxides: the case of the polar $\text{ZnO}(0001)$ surface, *Surf. Sci.* **486**, L502 (2001).
- [23] H. Li, L. K. Schirra, J. Shim, H. Cheun, B. Kippelen, O. L. A. Monti, and J.-L. Brédas, Zinc oxide as a model transparent conducting oxide: A theoretical and experimental study of the impact of hydroxylation, vacancies, interstitials, and extrinsic doping on the electronic properties of the polar $\text{ZnO}(0002)$ surface, *Chem. Mater.* **24**, 3044 (2012).
- [24] M. Valtiner, M. Todorova, and J. Neugebauer, Hydrogen adsorption on polar $\text{ZnO}(0001)$ -Zn: Extending equilibrium surface phase diagrams to kinetically stabilized structures, *Phys. Rev. B* **82**, 165418 (2010).
- [25] C. M. Schlepütz, Y. Yang, N. S. Hussein, R. Heinhold, H.-S. Kim, M. W. Allen, S. M. Durbin, and R. Clarke, The presence of a (1×1) oxygen overlayer on $\text{ZnO}(0001)$ surfaces and at Schottky interfaces, *J. Phys.: Condens. Matter* **24**, 095007 (2012).
- [26] L. L. Kelly, D. A. Racke, P. Schulz, H. Li, P. Winget, H. Kim, P. Ndione, A. K. Sigdel, J.-L. Brédas, J. J. Berry, S. Graham, and O. L. A. Monti, Spectroscopy and control of near-surface defects in conductive thin film ZnO, *J. Phys.: Condens. Matter* **28**, 094007 (2016).
- [27] L. K. Schirra, Charge transfer at metal oxide/organic interfaces, Doctoral thesis, The University of Arizona, 2012.
- [28] P. Herrmann and G. Heimel, Structure and stoichiometry prediction of surfaces reacting with multicomponent gases, *Adv. Mater.* **27**, 255 (2015).
- [29] See Supplemental Material at <http://link.aps.org/supplemental/10.1103/PhysRevMaterials.4.020602> for experimental and computational details as well as XPS, XSW, PhD, UPS, and LEED data [45–57].

- [30] D. P. Woodruff, Surface structure determination using x-ray standing waves, *Rep. Prog. Phys.* **68**, 743 (2005).
- [31] A. Gerlach, C. Bürker, T. Hosokai, and F. Schreiber, X-ray standing waves and surfaces X-ray scattering studies of molecule-metal interfaces, in *The Molecule-Metal Interface* (Wiley-Blackwell, Weinheim, Germany, 2013), Chap. 6, pp. 153–172.
- [32] M. Iachella, J. Cure, M. Djafari Rouhani, Y. Chabal, C. Rossi, and A. Estève, Water dissociation and further hydroxylation of perfect and defective polar ZnO model surfaces, *J. Phys. Chem. C* **122**, 21861 (2018).
- [33] C. Brülke, T. Heepenstrick, N. Humberg, I. Krieger, M. Sokolowski, S. Weiß, F. S. Tautz, and S. Soubatch, Long vertical distance bonding of the hexagonal boron nitride monolayer on the Cu(111) surface, *J. Phys. Chem. C* **121**, 23964 (2017).
- [34] S. Weiß, I. Krieger, T. Heepenstrick, S. Soubatch, M. Sokolowski, and F. S. Tautz, Determination of the adsorption geometry of PTCDA on the Cu(100) surface, *Phys. Rev. B* **96**, 075414 (2017).
- [35] G. van Straaten, M. Franke, F. C. Bocquet, F. S. Tautz, and C. Kumpf, Non-dipolar effects in photoelectron-based normal incidence x-ray standing wave experiments, *J. Electron. Spectrosc. Relat. Phenom.* **222**, 106 (2018).
- [36] F. Traeger, M. Kauer, C. Wöll, D. Rogalla, and H.-W. Becker, Analysis of surface, subsurface, and bulk hydrogen in ZnO using nuclear reaction analysis, *Phys. Rev. B* **84**, 075462 (2011).
- [37] A. Önsten, D. Stoltz, P. Palmgren, S. Yu, M. Göthelid, and U. O. Karlsson, Water adsorption on ZnO(0001): Transition from triangular surface structures to a disordered hydroxyl terminated phase, *J. Phys. Chem. C* **114**, 11157 (2010).
- [38] D. Woodruff, Normal incidence X-ray standing wave determination of adsorbate structures, *Prog. Surf. Sci.* **57**, 1 (1998).
- [39] V. Staemmler, K. Fink, B. Meyer, D. Marx, M. Kunat, S. G. Girol, U. Burghaus, and C. Wöll, Stabilization of Polar ZnO Surfaces: Validating Microscopic Models by using CO as a Probe Molecule, *Phys. Rev. Lett.* **90**, 106102 (2003).
- [40] P. Winget, L. K. Schirra, D. Cornil, H. Li, V. Coropceanu, P. F. Ndione, A. K. Sigdel, D. S. Ginley, J. J. Berry, J. Shim, H. Kim, B. Kippelen, J.-L. Brédas, and O. L. A. Monti, Defect-driven interfacial electronic structures at an organic/metal-oxide semiconductor heterojunction, *Adv. Mater.* **26**, 4711 (2014).
- [41] V. Lanzilotto, G. Lovat, G. Fratesi, G. Bavdek, G. P. Brivio, and L. Floreano, TiO₂(110) charge donation to an extended π -conjugated molecule, *J. Phys. Chem. Lett.* **6**, 308 (2015).
- [42] S. Duhm, C. Bürker, J. Niederhausen, I. Salzmann, T. Hosokai, J. Duvernay, S. Kera, F. Schreiber, N. Koch, N. Ueno, and A. Gerlach, Pentacene on Ag(111): Correlation of bonding distance with intermolecular interaction and order, *ACS Appl. Mater. Interfaces* **5**, 9377 (2013).
- [43] K. Nishidate and M. Hasegawa, Hydrogen-induced disruption of the ZnO(0001) polar surface, *Phys. Rev. B* **86**, 035412 (2012).
- [44] H. Ye, G. Chen, H. Niu, Y. Zhu, L. Shao, and Z. Qiao, Structures and mechanisms of water adsorption on ZnO(0001) and GaN(0001) surface, *J. Phys. Chem. C* **117**, 15976 (2013).
- [45] V. Blum, R. Gehrke, F. Hanke, P. Havu, V. Havu, X. Ren, K. Reuter, and M. Scheffler, Ab initio molecular simulations with numeric atom-centered orbitals, *Comput. Phys. Commun.* **180**, 2175 (2009).
- [46] J. P. Perdew, K. Burke, and M. Ernzerhof, Generalized Gradient Approximation Made Simple, *Phys. Rev. Lett.* **77**, 3865 (1996).
- [47] A. Tkatchenko and M. Scheffler, Accurate Molecular Van Der Waals Interactions from Ground-State Electron Density and Free-Atom Reference Data, *Phys. Rev. Lett.* **102**, 073005 (2009).
- [48] O. T. Hofmann, J.-C. Deinert, Y. Xu, P. Rinke, J. Stähler, M. Wolf, and M. Scheffler, Large work function reduction by adsorption of a molecule with a negative electron affinity: Pyridine on ZnO(10 $\bar{1}$ 0), *J. Chem. Phys.* **139**, 174701 (2013).
- [49] H. Karzel, W. Potzel, M. Köfferlein, W. Schiessl, M. Steiner, U. Hiller, G. M. Kalvius, D. W. Mitchell, T. P. Das, P. Blaha, K. Schwarz, and M. P. Pasternak, Lattice dynamics and hyperfine interactions in ZnO and ZnSe at high external pressures, *Phys. Rev. B* **53**, 11425 (1996).
- [50] D. C. Reynolds, D. C. Look, B. Jogai, C. W. Litton, G. Cantwell, and W. C. Harsch, Valence-band ordering in ZnO, *Phys. Rev. B* **60**, 2340 (1999).
- [51] T.-L. Lee and D. A. Duncan, A two-color beamline for electron spectroscopies at diamond light source, *Synchrotron Radiat. News* **31**, 16 (2018).
- [52] A. Franco-Cañellas, Q. Wang, K. Broch, D. A. Duncan, P. K. Thakur, L. Liu, S. Kera, A. Gerlach, S. Duhm, and F. Schreiber, Metal-organic interface functionalization via acceptor end groups: PTCDI on coinage metals, *Phys. Rev. Mater.* **1**, 013001 (2017).
- [53] S. Kera, T. Hosokai, and S. Duhm, Characteristics of organic-metal interaction: A perspective from bonding distance to orbital delocalization, *J. Phys. Soc. Jpn.* **87**, 061008 (2018).
- [54] D. P. Woodruff and A. M. Bradshaw, Adsorbate structure determination on surfaces using photoelectron diffraction, *Rep. Prog. Phys.* **57**, 1029 (1994).
- [55] D. P. Woodruff, Adsorbate structure determination using photoelectron diffraction: Methods and applications, *Surf. Sci. Rep.* **62**, 1 (2007).
- [56] J. Götzten and G. Witte, Rapid preparation of highly ordered ultraflat ZnO surfaces, *Appl. Surf. Sci.* **258**, 10144 (2012).
- [57] M. Timpel, M. V. Nardi, S. Krause, G. Ligorio, C. Christodoulou, L. Pasquali, A. Giglia, J. Frisch, B. Wegner, P. Moras, and N. Koch, Surface modification of ZnO(0001)-Zn with phosphonate-based self-assembled monolayers: Binding modes, orientation, and work function, *Chem. Mater.* **26**, 5042 (2014).